JOURNAL OF NATURAL PRODUCTS

pubs.acs.org/jnp

Article

Carboxylic Acid Tailoring in Thioquinolobactin Biosynthesis

Xuan Wang, Xiaolin Tian, Jiawei Guo, Fangyuan Cheng, Mingyu Liu, Shanmin Zheng, Yangliu Feng, Ying Lv, Yuanning Li, Shengying Li, and Xingwang Zhang*

Cite This: *J. Nat. Prod.* 2025, 88, 1425−1433

Read Online

ACCESS | Metrics & More | Article Recommendations | Supporting Information

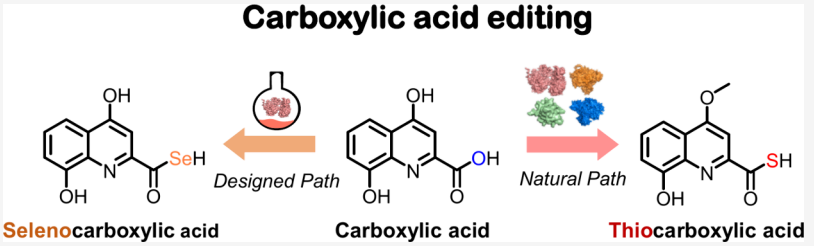

ABSTRACT: The biosynthetic mechanism underlying the formation of thiocarboxylic acid moieties in natural products remains largely unknown. Thioquinolobactin (TQB) is a *Pseudomonas fluorescens* derived siderophore that contains a thiocarboxylic acid moiety within its structure. Although the biosynthetic gene cluster and proposed pathway for TQB formation have been reported, the biosynthetic mechanism related to the thiocarboxylic acid formation are yet to be fully understood. In this study, we address this question by demonstrating that a unique dual-domain protein QbsL, which possesses both CoA ligase and methyltransferase activities, along with the sulfurtransferase QbsK, facilitates the assembly of the thiocarboxylic acid. Based on this mechanism, we develop a chemoenzymatic method to convert carboxylic acid into selenocarboxylic acid, thereby generating selenium-containing analogues of TQB. These findings resolve the long-standing mystery in TQB biosynthesis and expand the synthetic toolkit for carboxylic acid modification.

Sulfur-containing natural products represent a diverse and significant class of bioactive compounds, playing important roles in physiological metabolisms, ecological interactions, and human disease treatment.[1−3] To date, more than a thousand sulfur-containing natural products have been discovered, encompassing a wide range of structural forms, including sulfides, thiols, sulfates, and thioacids.[4,5] Thiocarboxylic acid-containing natural products, such as thioquinolobactin (TQB),[6] thioplatensimycin (thioPTM),[7] and 2,6-pyridinedithiocarboxylic acid (Figure 1A),[8,9] are rare in nature. These compounds typically exhibit biological activities, including antibacterial and antifungal effects. However, due to their rarity and inherent instability, the biosynthetic mechanisms of thiocarboxylic acid-containing natural products remain largely unexplored. To our knowledge, thioPTM and sulfenicin are the only examples for which the biosynthetic mechanism of thiocarboxylic acid formation has been elucidated (Figure 1B and 1C).[7,10]

TQB is a siderophore produced by *Pseudomonas fluorescens*, utilizing the phenoxide oxygen atom, pyridine nitrogen atom, and thiocarboxylic acid group as ligands for ferric iron chelating (Figure 2).[11] In addition to the ferric iron scavenging ability, TQB exhibits antifungal activity and demonstrates potent inhibitory efficacy against *Pythium* spp., which are a group of soil-inhabiting oomycetes that could cause devastating root diseases in greenhouse -grown crops,[12,13] making it a potential biocontrol agent.[14] The biosynthetic gene cluster (BGC) of TQB, namely *qbs*, was first reported by the Cornelis group,[6] which also proposed a putative biosynthetic pathway (Figures 2A and B). In a later study, the Begley group reported that TQB employs a variant of the sulfur incorporation chemistry found in thiamine and molybdopterin biosynthesis. Specifically, it utilizes the thiolated sulfur carrier protein (SCP) QbsE (i.e., QbsE-COS$^-$) as the sulfur donor (Figure 2C).[15] However, the enzymatic basis and catalytic specifics governing sulfur transfer from QbsE-COS$^-$ to the proposed acceptor substrate, xanthurenic acid (XTA), remain unknown. Herein, we address these outstanding questions through *in vitro* characterization of the key enzymes involved in the formation of the thiocarboxylic acid group in the TQB.

Selenium (Se) is positioned in the same group of the Periodic Table of Elements as sulfur and shares similar, yet distinct, physical and chemical properties.[16] In comparison to organosulfur compounds, organoselenium compounds demonstrate advantages in enhancing antioxidant activities, fine-tuning drug metabolism, and combating drug resistance.[17,18]

Received: March 15, 2025
Revised: May 28, 2025
Accepted: May 30, 2025
Published: June 11, 2025

https://doi.org/10.1021/acs.jnatprod.5c00331
J. Nat. Prod. 2025, 88, 1425−1433

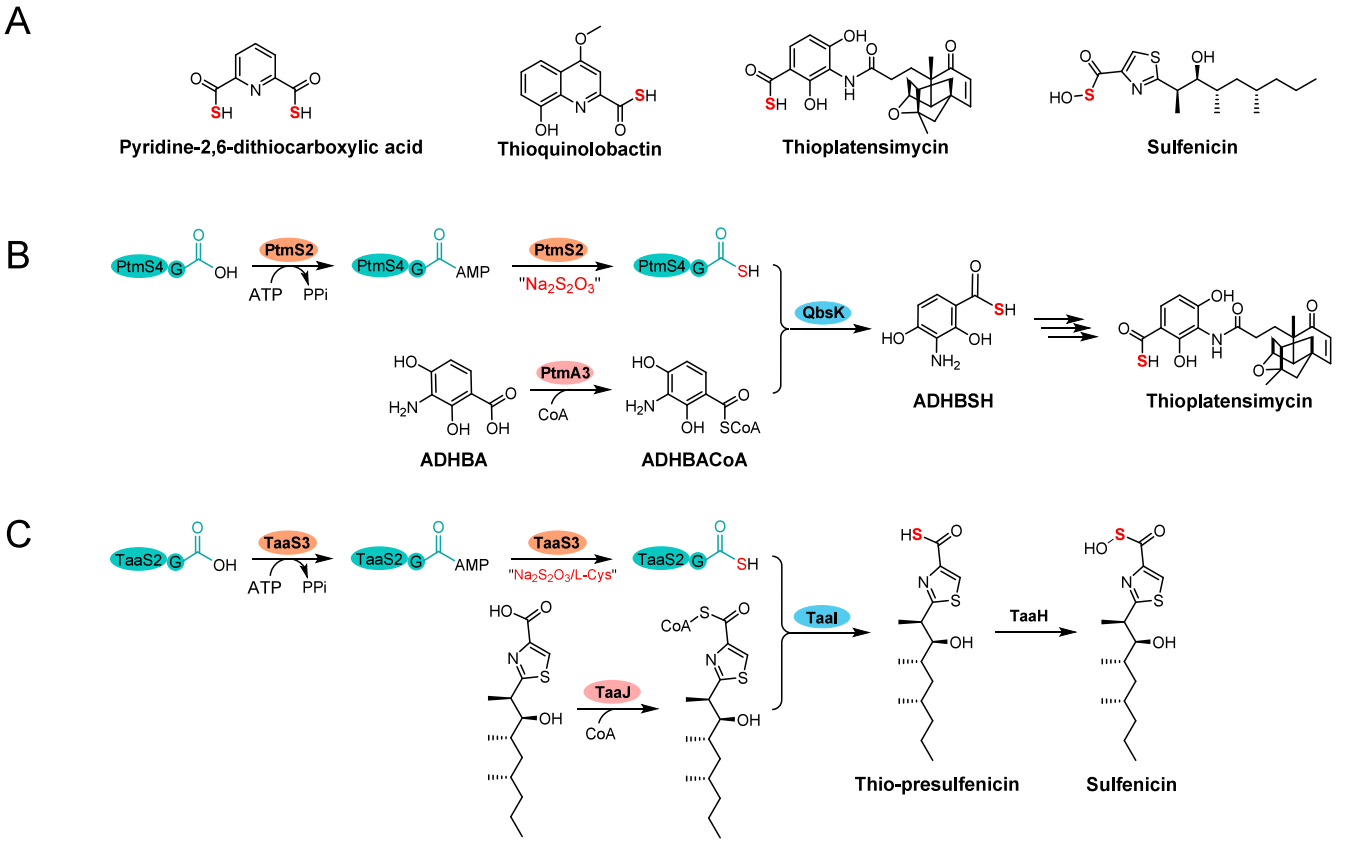

Figure 1. Representative thiocarboxylic acid containing natural products and related biosynthetic pathways: (A) Representative thiocarboxylic acid containing natural products; (B) biosynthetic route of the thiocarboxylic acid moiety in thioplatensimycin (thioPTM); (C) biosynthetic route of the thiocarboxylic acid moiety in sulfenicin.

Despite the development of many chemical synthetic methods for organoselenium compounds, biosynthesis of these compounds is still in its infancy.[19−22] In a previous study, we developed a SCP mediated C−Se bond formation method to produce organoselenium compounds.[23] In this study, based on the sulfur incorporation mechanism of TQB, we explored to develop a SCP-free method for producing the selenometabolites, thereby expanding the synthetic toolkit for generating organoselenium compounds.

RESULTS AND DISCUSSION

Reconstitution of the TQB Biosynthetic Pathway *In Vitro*. In the previously proposed biosynthetic pathway (Figure 2B),[6] TQB was suggested to be produced through an adenosine monophosphate (AMP)-activated intermediate generated by the dual-domain protein QbsL, with XTA serving as the substrate. In 2018, the Shen group revealed the biosynthetic pathway of thioPTM, in which the thiocarboxylic acid formation involves a coenzyme A (CoA)-activated intermediate (Figure 1B).[7] In this route, the acyl-CoA synthetase PtmA3 activates the substrate ADHBA, leading to the formation of ADHB-CoA. This CoA-ester is subsequently converted to the thiocarboxylic acid-containing product ADHBSH under the catalysis of a type III CoA-transferase PtmU4, using the thiolated SCP PtmS2-COS$^-$ as sulfur donor (Figure 1B).[7] Recently, the Moore and Li group reported the biosynthetic pathway of sulfenicin, in which the formation of the thiocarboxyl group employs a similar strategy (Figure 1C).[10]

In the *qbs* cluster, *qbsK* is also predicted to encode a type III CoA-transferase, aligning PtmU4 and TaaI in the thioPTM and sulfenicin pathways (Figure 2A). Protein structural model (generated by AlphaFold2[24]) alignment reveals a high structural similarity between QbsK and PtmU4/TaaI, with a root-mean-square deviation (RSMD) value of 1.496/1.062, despite their relatively low sequence identity (35.17% for QbsK and 44.94% for TaaI, Figure S1). Given the strong correlation between protein structures and functions, we proposed that TQB might use a biosynthetic strategy for the thiocarboxylic acid moiety similar to thioPTM and sulfenicin instead of the previously hypothesized AMP-dependent pathway.

To test our hypothesis, we sought to reconstitute the biosynthetic pathway of TQB *in vitro*. All relevant protein-encoding genes, including *qbsC*, *qbsK*, *qbsL*, and *qbsE** (a modified version of *qbsE* with deletion of codons encoding the C-terminal CF dipeptide motif to circumvent QbsD-mediated hydrolysis[15]), were cloned from the genomic DNA of *P. fluorescens* ATCC 17400 (Table S4). The corresponding proteins were then expressed and purified to homogeneity using *E. coli* BL21(DE3)/Rosetta(DE3) or *P. fluorescens* ATCC 17400 as the hosts (Figures S2 and S3). First, we reconstituted the thiolation process of CF-truncated SCP QbsE*.

When QbsE*-COO$^-$ was incubated with the MoeZ-like activating enzyme QbsC in the presence of ATP, $MgCl_2$, and $Na_2S_2O_3$, the expected QbsE*-COS$^-$ species was formed, as confirmed by high resolution electrospray ionization mass spectrometry (HRESI-MS) analysis (Figure 3A).

https://doi.org/10.1021/acs.jnatprod.5c00331
J. Nat. Prod. 2025, 88, 1425−1433

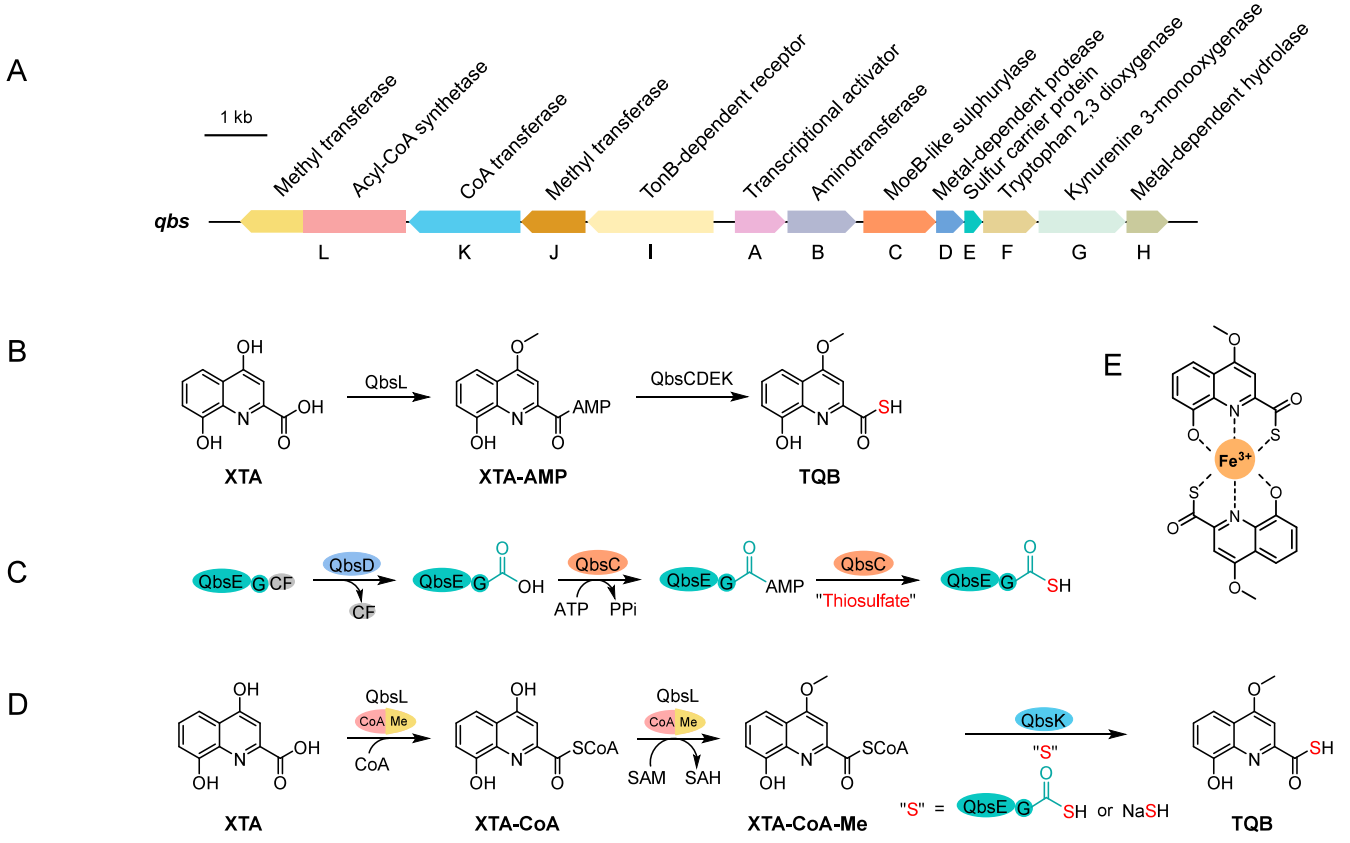

Figure 2. Thioquinolobactin (TQB) biosynthesis and iron chelation. (A) TQB biosynthetic gene cluster from *P. fluorescens* ATCC 17400; (B) previously proposed biosynthetic pathway for TQB; (C) previously identified sulfur carrier protein (SCP) thiolation pathway, in which the sulfur "S" is derived from thiosulfate; CF represents a dipeptide motif at the QbsE *C*-terminus, which is cleaved by the metal-dependent hydrolase QbsD to expose the GG-tail for subsequent sulfurization; (D) elucidated biosynthetic pathway for TQB in this study; (E) proposed ferric iron complex of TQB.

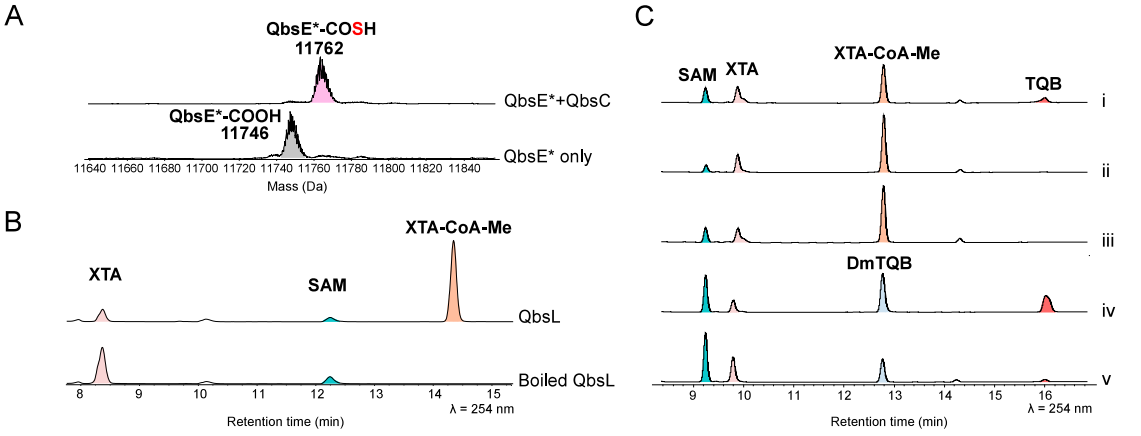

Figure 3. *In vitro* reconstitution of TQB biosynthesis. (A) HRESI-MS analysis revealed the conversion of QbsE*-COOH (*calc.* 11746 Da) into the activated form QbsE*-COSH (*calc.* 11762 Da) after 30 min of incubation with QbsC, ATP, $MgCl_2$, and $Na_2S_2O_3$. (B) HPLC analysis of QbsL-mediated reaction (containing QbsL, XTA, ATP, $MgCl_2$, CoA and SAM) with boiled QbsL as a negative control. (C) *In vitro* reconstitution of TQB. (i) Sulfur transfer reaction using QbsE* as the sulfur donor (containing QbsE, QbsC, QbsL, QbsK, XTA, ATP, $MgCl_2$, CoA, $Na_2S_2O_3$, and SAM); (ii) negative control for (i) with boiled QbsE*; (iii) negative control for (i) with boiled QbsK; (iv) sulfur transfer reaction using NaSH as sulfur donor (containing QbsL, QbsK, XTA, ATP, $MgCl_2$, CoA, NaSH, and SAM); (v) negative control for (iv) with boiled QbsK. *Note*: (a) DmTQB shares an identical retention time with XTA-CoA-Me, and is identified by HRESI-MS/MS (Figure S6) and NMR analysis (Figures S15–S19); (b) SAM and XTA showed reversed elution orders in panels B and C are attributed to the use of different HPLC mobile phases: ACN/H_2O (both containing 0.1% formic acid, Panel A) vs ACN/H_2O (with H_2O containing 10 mM ammonium acetate, Panel B).

QbsL is predicted to be a dual-domain protein, consisting of an AMP/CoA-binding domain and an *S*-adenosyl methionine (SAM)-binding domain (Figure 4A). The AMP/CoA-binding domain containing proteins typically function as AMP- or CoA-ligases involving in various physiological processes.[25−27] SAM-dependent methyltransferases, as predicted for the QbsL-

https://doi.org/10.1021/acs.jnatprod.5c00331
J. Nat. Prod. 2025, 88, 1425−1433

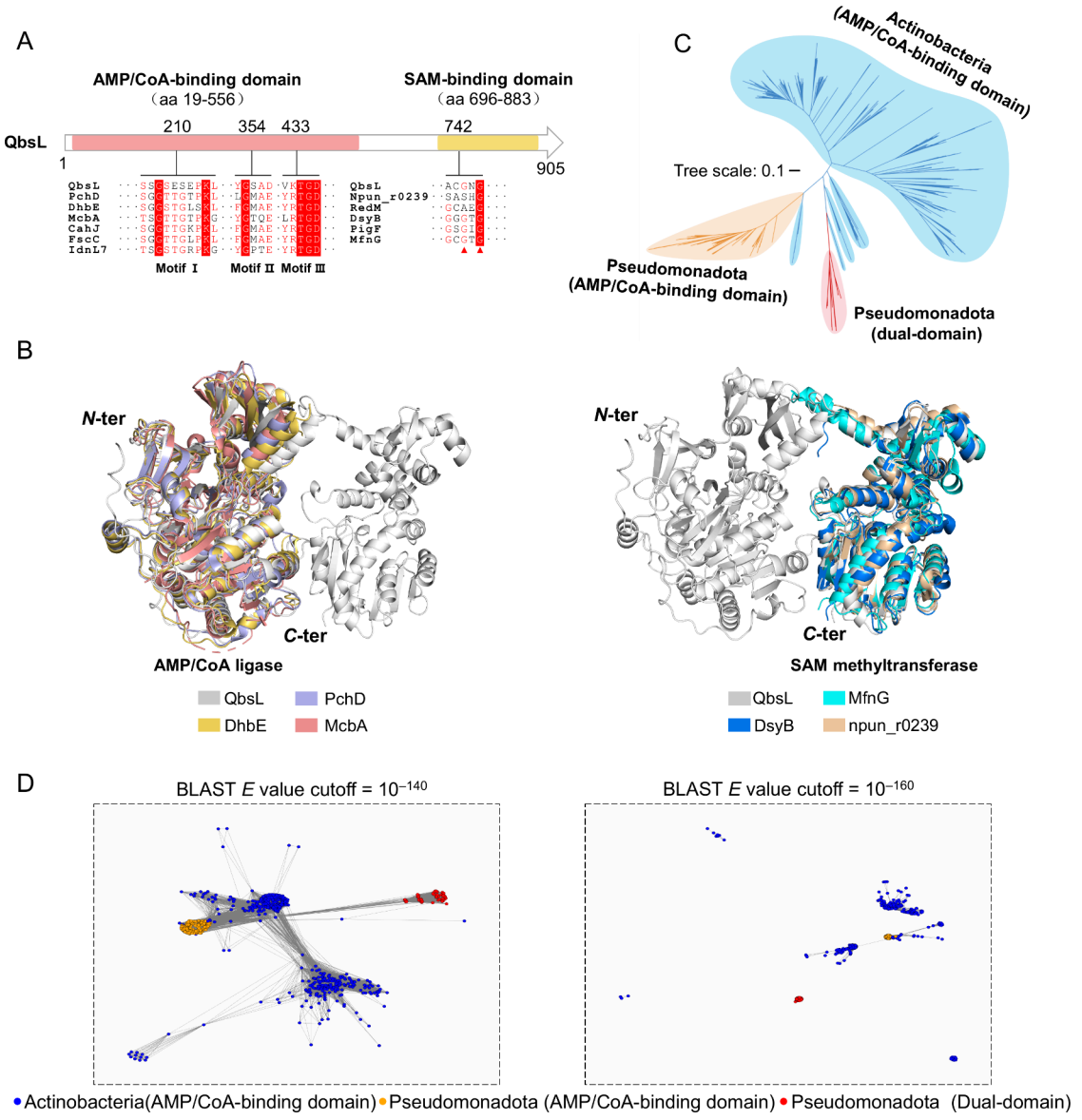

Figure 4. Bioinformatics analysis of *qbsL*-like genes from bacteria. (A) Architecture of the dual-domain protein QbsL and its conserved motifs (for more details, please see Figures S21, S22 and Table S6). (B) Structural comparison of QbsL with crystallized AMP-dependent adenylating enzymes (left: PchD 7tz4, DhbE 1mdf, McbA 6sq8) and SAM-dependent methyltransferases (right: MfnG 7ux6, DsyB 7wdq, npun_r0239 2r3s).The protein structure model of QbsL was predicted by Alphafold 3.[29] (C) Phylogenetic tree of QbsL homologues, with Pseudomonadota (red/orange) and Actinobacteria (blue) branches highlighted. (D) Sequence similarity network analysis of QbsL with its homologous proteins.

associated domain, usually use SAM as a methyl donor to methylate their substrates.[28] Structural alignment reveals that the 3D structures of the AMP/CoA-binding and SAM-binding domains in the QbsL model, generated by AlphaFold3,[29] closely resemble the crystal structures of related AMP/CoA-ligases and SAM-methyltransferases, respectively (Figures 4B, S4 and S5). This observation raises an important question regarding the catalytic sequence of this dual-function enzyme.

To address this question, we first reconstituted the catalytic activity of QbsL *in vitro*. Co-incubation of XTA and QbsL in the presence of ATP, SAM, CoA, and $MgCl_2$ led to the formation of a CoA-tethered and methylated XTA product (Figure 3B). The identity of this product was determined as XTA-CoA-Me (Figure 2D) based on HRESI-MS/MS analysis (Figure S6) and biosynthetic logic. However, no product was detected in the negative control with boiled QbsL. These results confirmed the dual functions of QbsL in CoA ligation and methylation. Next, we separately expressed the single-domain proteins $QbsL_{CoA}$ and $QbsL_{Me}$ (Figure S3). Replacing the intact QbsL with $QbsL_{CoA}$ or $QbsL_{Me}$ in the reaction mixture showed that the reaction with $QbsL_{CoA}$ produced the XTA-CoA intermediate, while no product was generated with $QbsL_{Me}$ (Figures S6 and S7). These results established that the CoA ligation step precedes the methylation step in the catalytic order of the reaction.

To explore if there is any mutual interference between the two domains of QbsL, we separately compared the substrate (XTA) conversion ratios of the full length QbsL and the single domain protein $QbsL_{CoA}$ in a time-course assay. The results revealed that QbsL achieved 96.9% substrate−conversion within 30 min, while $QbsL_{CoA}$ showed significantly lower substrate−conversion ratios throughout the experimental time frame (Figure S8). Notably, when XTA was coincubated with both single-domain proteins ($QbsL_{CoA}$ and $QbsL_{Me}$) simulta-

https://doi.org/10.1021/acs.jnatprod.5c00331
J. Nat. Prod. 2025, 88, 1425−1433

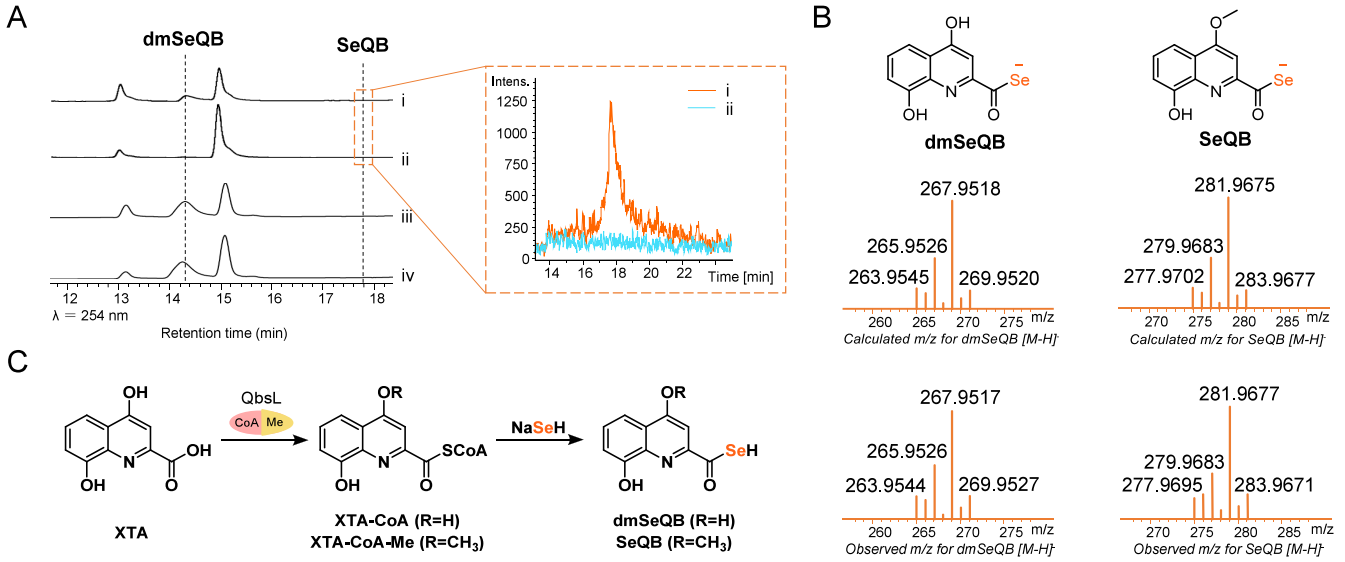

Figure 5. Selenocarboxylic acids production and characterization. (A) HPLC and HPLC-MS analysis of selenocarboxylic acid production reactions. (i) Co-incubation of QbsL, QbsK, NaSeH (2 mM), XTA, $MgCl_2$, ATP, SAM, CoA and DTT; (ii) negative control for (i) with boiled QbsK; (iii) reaction with 20 mM NaSeH; (iv) negative control for (iii) with boiled QbsK (20 mM NaSeH) . (B) Observed and calculated mass spectra of SeQB and dmSeQB; (C) chemoenzymatic synthesis scheme for selenocarboxylic acid production.

neously, the substrate−conversion ratio increased to a level comparable to that achieved by the full-length QbsL (Figure S9). These results together suggested that there is synergistic interference between the two domains. Substrate tunnel calculations of the full length QbsL indicate that a cascade tunnel might form between the two domains of QbsL to facilitate intermediate channeling, thereby enhancing the efficiency of the whole catalytic pathway (Figure S10).

Following the activation of both the SCP (from QbsE*-COO^- to QbsE*-COS^-) and the substrate (from XTA to XTA-CoA-Me), we further investigated the sulfurtransfer process through a one-pot reaction. Specifically, XTA was incubated with QbsE*, QbsC, QbsL, QbsK, SAM, CoA, ATP, $Na_2S_2O_3$ and $MgCl_2$ for 2 h. HPLC-HRESI-MS/MS analysis of the reaction mixture revealed TQB formation (Figures 3C and S6), as evidenced by nuclear magnetic resonance (NMR) spectroscopic analysis of the purified product (Figures S11−S14). Omission of QbsE* or QbsK abolished the formation of TQB (Figure 3C).

Furthermore, substitution of the native sulfur donor QbsE*-COS^-, generated by the coincubation of QbsE*, QbsC, $Na_2S_2O_3$, and ATP, with sodium hydrosulfide (NaSH) led to an increased production of TQB (Figure 3C). Intriguingly, this reaction also yielded the demethylated analogue of TQB, namely, dmTQB, as confirmed by NMR analysis (Figures S15−S19), with a ratio of 2.11:1 relative to TQB. The formation of dmTQB is attributed to the ability of SH^- to directly convert the XTA-CoA intermediate into dmTQB before its methylation. The absence of active QbsK in the NaSH-supported reaction did not completely abolish the formation of TQB and dmTQB but reduced their yields (TQB production dropped to 4.7% of the initial yield; Figure 3C). Additionally, we enzymatically synthesized the XTA-CoA-Me intermediate and incubated it with QbsK to test whether it serves as the direct substrate for the sulfur-transfer reaction. As expected, the final product TQB was formed (Figure S20), thus demonstrating that XTA-CoA-Me should be the real intermediate involved in TQB biosynthesis. These results together suggest that QbsK can use both QbsE*-COS^- and free SH^- as sulfur donors to mediate the sulfurtransfer reactions from XTA-CoA-Me, and that the activated XTA-CoA-Me can also be converted to TQB by SH^- slightly and spontaneously. Collectively, these results confirmed that QbsK is the sulfurtransferase involved in TQB biosynthesis, with the capability of utilizing different forms of sulfur donors.

Evolutionary Analysis of QbsL. Although numerous AMP/CoA ligases and SAM-dependent methyltransferases have been identified,[25−27,30] QbsL represents the first known example of a naturally occurring, fused dual-domain enzyme. To explore the distribution and evolutionary origin of QbsL-like proteins, we analyzed 43,815 bacterial genomes from the NCBI Reference Sequence Database, encompassing 42 bacterial phyla, thereby ensuring comprehensive taxonomic representation for our analyses (Supplementary table). This led to the identification of 52 genes encoding QbsL-like dual-domain proteins, all from Pseudomonadota strains (Table S5). Phylogenetic analysis showed that *qbsL* homologous genes form a separate clade (Figure 4C). They are distinct from the actinobacterial single-domain AMP/CoA-ligase genes but share a common origin. Sequence similarity network, constructed with an e-value threshold of 10^{-140}, revealed that the *qbsL*-like fused genes are directly connected to those actinobacterial AMP/CoA-ligase encoding genes (Figure 4D). This finding and the phylogenetic tree support the notion that the fused genes exhibit notable similarity to the nonfused actinobacterial AMP/CoA-ligase genes (Figure 4D). Meanwhile, the similarity network with an e-value of 10^{-160} indicated that nonfused Pseudomonadota genes and actinobacterial genes cluster together (Figure 4D). This suggests a high degree of similarity between them.

Interestingly, neighboring gene analysis revealed that all 52 *qbsL*-like fused genes are located adjacent to other TQB biosynthetic genes (Table S5). In other words, within the scope of our analysis, *qbsL*-like genes represent a specific class of genes dedicated to TQB production in the Pseudomonadota strains. This finding is also supported by a recent study in

https://doi.org/10.1021/acs.jnatprod.5c00331
J. Nat. Prod. 2025, 88, 1425−1433

which the authors found that the TQB BGC is widely distributed among *Pseudomonas* strains.[31] Since siderophores enhance iron uptake under low-iron conditions, we propose that the *qbsL*-like genes have evolved to help Pseudomonadota strains gain a growing advantage under extreme conditions.[32] The associated gene clusters likely function as an adaptive strategy, facilitating rapid and efficient responses to fluctuations in the environmental iron availability.

Chemoenzymatic Synthesis of Selenocarboxylic Acids. After elucidating the biosynthetic mechanism of the thiocarboxylic group, we turned to exploring the production of the selenocarboxylic acid analogue of TQB using this biosynthetic machinery. Based on our observations that the sulfurtransferase QbsK can directly utilize SH^- as a sulfur donor to produce TQB, and that SH^- can directly convert XTA-CoA-Me into TQB, we investigated whether this system could similarly use SeH^- to generate selenoquinolobactin (SeQB).

NaSeH was prepared by reducing selenium powder (Se^0) with sodium borohydride ($NaBH_4$) under nitrogen (N_2) atmosphere.[33] XTA was incubated with QbsL, QbsK, ATP, SAM, CoA, $MgCl_2$, and DTT in the presence of freshly prepared NaSeH at 30 °C for 30 min. When the concentration of NaSeH was 2 mM, HPLC-HRESI-MS/MS analysis of the reaction mixture revealed the formation of a trace amount of SeQB (with a yield less than 1%) (Figures 5A, B and S6), as evidenced by the isotopic pattern analysis with the calculated data. Interestingly, a substantial amount of a demethylated derivative, dmSeQB, was detected in an approximate yield of 3.69% (Figures 5A and S6). The omission of QbsK in the negative control reaction led to a significant reduction in the production of both SeQB and dmSeQB (Figure 5A). The formation of dmSeQB was attributed to the direct conversion of the XTA-CoA intermediate before its methylation, owing to the strong nucleophilicity of SeH^-. This hypothesis was supported by the observation that increasing NaSeH concentration from 2 to 20 mM significantly enhanced dmSeQB yield from 3.69% to approximately 13.46% in both QbsK-present and QbsK-absent reactions (Figure 5A). This suggests that the QbsL-mediated reaction with 20 mM NaSeH, without QbsK participation, may represent a simpler and more practical method for synthesizing selenocarboxylic-acid-containing compounds (Figure 5C). Next, we attempted to purify SeQB and dmSeQB as product standards to measure their chemical and biological properties. However, obtaining sufficient quantities proved challenging due to the low yield and intrinsic instability of the compounds, with complete degradation occurring within 24 h at room temperature and within 3 days at 4 °C (Figures S23 and S24). Together, we presented a new two-step chemoenzymatic method to convert the carboxyl acid group (R-COOH) into the selenocarboxyl acid group (R-COSeH) using a single enzyme without any group to be protected (Figure 5C). Consequently, our results establish a chemoenzymatic method for selenocarboxylic acid production.

CONCLUSION

In summary, we elucidated the enzymatic basis and catalytic specifics regarding the formation of the thiocarboxylic acid moiety in the TQB biosynthesis. Our results demonstrate that TQB employs a unique and specific dual-domain protein, QbsL, along with three other enzymes to facilitate the assembly of the thiocarboxylic acid group by using different types of sulfur sources. QbsL represents the first example of a naturally occurring, fused dual-function enzyme that integrates CoA ligation and *O*-methylation activities. Moreover, based on the mechanism for thiocarboxylic acid biosynthesis, we synthesized the selenocarboxylic acid derivatives of TQB via a chemo-enzymatic approach. Given the widespread distribution of CoA ligases in nature, this method may offer a general approach for synthesizing selenium analogs of thiocarboxylic acid compounds. This work enriches the (bio)synthetic toolkit for carboxylic acid modification, enabling the conversion of a carboxylic acid group into either a thiocarboxylic acid or a selenocarboxylic acid group.

EXPERIMENTAL SECTION

General Experimental Procedures. HPLC analyses for small-molecule products were conducted using a YMC-Triart C18 column (250 × 4.6 mm, 5 μm) with a biphasic solvent system consisting of acetonitrile (ACN) and water (containing 0.1% formic acid or 10 mM NH_4OAc) on a Thermo HPLC system. Semipreparative HPLC was performed on a Thermo HPLC system equipped with a Pack Pro C18 column (10 mm × 250 mm × 5 μM, YMC, Japan). HPLC-HRESI-MS/MS analyses were carried out using a Bruker Impact HD High-Resolution Q-TOF mass spectrometer. For HPLC-ESI-MS analysis of proteins, a Thermo High-Resolution LTQ-Orbitrap mass spectrometer with ETD was employed. Nuclear magnetic resonance (NMR) spectra were recorded on a Bruker AVANCE III 600 spectrometer. NMR data were processed using MestReNova 9.0.

Materials. Antibiotics and CoA used in this study were purchased from Solarbio (Beijing, China). ATP and IPTG were purchased from Aladdin (Shanghai, China). XTA, SAM and L-Rhamnose monohydrate were purchased from McLean (Shanghai, China). Other chemicals and reagents were purchased from Sinopharm Chemical Reagent Co., Ltd. (Shanghai, China). PCR primers and DNA sequencing were ordered from Sangon Biotech (Shanghai, China). The enzymes used in cloning experiments were obtained from Fisher Scientific (PA, USA) and were employed according to the manufacturer's protocols. The Ni-NTA Sefinose Resin (Settled Resin) for protein purification was acquired from Sangon Biotech (Shanghai, China). DNA gel extraction and plasmid preparation kits were purchased from Omega Bio-Tek, Inc. (GA, USA). Growth medium components were bought from Hope Bio-Technology Co., Ltd. (Qingdao, China).

Strains and Culture Conditions. The strains, plasmids, and primers used in this study are listed in Tables S1−S3. *Pseudomonas fluorescens* ATCC 17400 was purchased from the China General Microbiological Culture Collection Center (CGMCC). *P. fluorescens* ATCC 17400 was grown in lysogenyl broth (LB) at 30 °C and 220 rpm for genomic DNA isolation. *Escherichia coli* was grown in lysogeny broth (LB) at 37 °C while being shaken at 220 rpm, with appropriate antibiotic selection applied as necessary. *E. coli* DH5α strain was used for vector construction and plasmid preparation. *E. coli* BL21(DE3), *E. coli* Rosetta(DE3) and *P. fluorescens ATCC* 17400 strains were used for protein expression.

Molecular Cloning. The *qbsE** (with the CF motif-encoding codons removed), *qbsC*, *qbsL*, $qbsL_{CoA}$ (Gene fragment of the AMP/CoA-binding domain), $qbsL_{Me}$ (Gene fragment of the SAM-binding domain) and *qbsK* genes were amplified by PCR from the genomic DNA of *P. fluorescens* ATCC 17400 strain with 2 × Phanta Flash Master Mix (Vazyme Biotech, Nanjing, China). The encoding ORFs of QbsE* and QbsC were cloned into the *Nco*I/*Hind*III-digested pET28b to yield the expression vectors for production of the *N*-terminal His_6-tagged proteins using a ClonExpress II One Step Cloning Kit (Vazyme Biotech, Nanjing, China). The encoding ORFs of QbsL, $QbsL_{CoA}$ and $QbsL_{Me}$ were cloned into the *BamH*I/*Hind*III-digested pET28a-SUMO to yield the expression vectors for production of the *N*-terminal SUMO-His_6-tagged proteins. The encoding ORF of QbsK was cloned into the *Nde*I/*Hind*III-digested pBBR1 to generate an expression vector for the *N*-terminal His_6-

https://doi.org/10.1021/acs.jnatprod.5c00331
J. Nat. Prod. 2025, 88, 1425−1433

tagged protein. The above plasmid vectors were transformed into *E. coli* DH5α for plasmid amplification. The recombinant plasmids were verified by DNA sequencing, and the correct plasmids were chemically transformed into *E. coli* BL21 (DE3)/*E. coli* Rosetta(DE3) or *P. fluorescens* for protein overexpression.

Protein Expression and Purification. A single colony of recombinant *E. coli* BL21(DE3) or *P. fluorescens* that harbors the expression vector of target protein was cultivated in 5 mL of lysogeny broth (LB) supplemented with 50 mg/L kanamycin, while the engineered *E. coli* Rosetta(DE3) strains were grown in 5 mL of LB containing 25 mg/L kanamycin and 34 mg/L chloramphenicol. The culture was incubated at 220 rpm and 37 °C for 16 h. The resulting seed culture was inoculated into 0.5 L LB medium (in a 2 L conical flask) supplemented with either 50 mg/L kanamycin (for *E. coli* BL21(DE3) and *P. fluorescens*) or 25 mg/L kanamycin plus 34 mg/L chloramphenicol (for *E. coli* Rosetta(DE3)). The culture was then incubated at 37 °C with shaking at 220 rpm until OD_{600} reached 0.6−0.8. Then, protein expression was induced by the addition of 0.25 mM isopropyl-D-thioga-lactopyranoside (IPTG) (*E. coli* strains) or 15g/L rhamnose (*P. fluorescens* strains), and the cells were grown for another 18−20 h at 18 °C with shaking. After harvesting the cells by centrifugation at 6000×*g* for 10 min at 4 °C, the pellet was resuspended in lysis buffer (50 mM NaH_2PO_4, 300 mM NaCl, 10 mM imidazole, 10% glycerol, pH 8.0), lysed by sonication, and centrifuged at 10,000×*g* for 60 min at 4 °C. The supernatant was mixed with Ni-NTA resin (Qiagen, Venlo, Netherlands) and incubated with gentle mixing for 0.5 h. Then, the resin with bound proteins was washed with 100−300 mL of precooled wash buffer (50 mM NaH_2PO_4, 300 mM NaCl, 20 mM imidazole, and 10% glycerol, pH 8.0). Finally, the target His_6-tagged proteins were eluted with 5−10 mL of elution buffer (50 mM NaH_2PO_4, 300 mM NaCl, 250 mM imidazole, 10 glycerol, pH 7.4). The resultant protein with an *N*-terminal His_6-tag was desalted using a PD-10 column (GE Healthcare, Buckinghamshire, UK), and concentrated using an Amicon Ultra centrifugal filter of appropriate molecular weight cutoff (Merck KGaA, Darmstadt, Germany) in desalting buffer (50 mM NaH_2PO_4, 100 mM NaCl, 10% glycerol, pH 7.4). The purified proteins were stored at −80 °C for later use. Protein concentrations were determined with Thermo NanoDrop equipment.

Enzymatic Activity of QbsE* and QbsC. The sulfur carrier protein activation reactions were performed in the reaction buffer (50 mM NaH_2PO_4, 300 mM NaCl, and 10% glycerol, pH = 7.4), and the reaction mixture contained 1 mM ATP, 2 mM $Na_2S_2O_3$, 5 mM $MgCl_2$, 20 μM QbsE* and 10 μM QbsC in a total volume of 50 μL. After incubation at 30 °C for 30 min, the reaction was quenched with liquid nitrogen, centrifuged at 4 °C, and the supernatants were analyzed by HPLC-ESI-MS using a gradient elution program of ACN in H_2O (0.1% formic acid) with a C4 column at the positive ion mode. The HPLC program was set as follows: 0−3 min, 5% (ACN/H_2O); 3−15 min, 5−90%; 15−18 min, 90%; 18−19 min, 90−5%; and 19−25 min, 5% at a flow rate of 1 mL/min, with UV monitoring at 280 nm. Electrospray ionization (ESI) in positive ion mode was employed with the following source parameters: capillary voltage, 3500 V; nebulizer pressure, 0.5 bar; dry gas flow, 6.0 L/min; and dry gas temperature, 200 °C.

Enzymatic Activity of QbsL. The reaction contained 200 μM XTA, 10 μM QbsL, 3 mM ATP, 5 mM $MgCl_2$, 2 mM SAM, 1 mM CoA was performed in reaction buffer (50 mM NaH_2PO_4, 300 mM NaCl, and 10% glycerol, pH = 7.4) in a total volume of 100 μL. The mixture was incubated for 30 min at 30 °C. The reaction was then quenched with 200 μL of methanol and centrifuged, and the supernatants were analyzed with HPLC or HPLC-MS. The HPLC program, utilizing ACN in H_2O (10 mM ammonium acetate), was set as follows: 0−1 min, 5%; 2−25 min, 5−60%; 25−26 min, 60−100%; 26−30 min, 100%; 30−31 min, 100−5%; and 31−35 min, 5% at a flow rate of 1 mL/min, monitoring at 254 nm.

Time-Course Assay for QbsL- and $QbsL_{CoA}$-Catalyzed Reactions. The time-course experiments were performed in 100 μL reaction volumes containing 200 μM XTA, 2 mM SAM, 1 mM CoA, 4 mM ATP, 5 mM $MgCl_2$, and 10 μM QbsL/$QbsL_{CoA}$ in reaction buffer (50 mM NaH_2PO_4, 300 mM NaCl, and 10% glycerol, pH 7.4). Both sets of reactions were incubated at 30 °C and quenched at 1, 5, 10, 30, and 60 min for HPLC analysis. The HPLC program, utilizing ACN in H_2O (10 mM ammonium acetate), was set as follows: 0−1 min, 5% (ACN/H_2O); 2−25 min, 5−60%; 25−26 min, 60−100%; 26−30 min, 100%; 30−31 min, 100−5%; and 31−35 min, 5% at a flow rate of 1 mL/min, monitored at 254 nm.

Enzymatic Activity of QbsK. The SCP-mediated one-pot reaction contained 200 μM XTA, 10 μM QbsE*, 5 μM QbsC, 10 μM QbsL, 5 μM QbsK, 2 mM SAM, 500 μM CoA, 4 mM ATP, 2 mM $Na_2S_2O_3$ and 5 mM $MgCl_2$. The mixtures were coincubated at 30 °C for 2 h. Then, 200 μL of methanol were added to quench the reaction. The supernatants were analyzed by using HPLC-MS with a gradient elution program following centrifugation. The HPLC program, utilizing ACN (0.1% formic acid) in H_2O (0.1% formic acid), was set as follows: 0−1 min, 5%; 2−25 min, 5−60%; 25−26 min, 60−100%; 26−30 min, 100%; 30−31 min, 100−5%; and 31−35 min, 5% at a flow rate of 1 mL/min, monitoring at 254 nm.

The NaSH-mediated one-pot reaction contained 200 μM XTA, 5 mM NaSH, 4 mM ATP, 5 mM $MgCl_2$, 2 mM SAM, 500 μM CoA, 10 μM QbsL and 5 μM QbsK in phosphate buffer (50 mM, pH 7.4). The mixtures were coincubated at 30 °C for 2 h. Then, 200 μL of methanol was added to quench the reaction. The HPLC analysis method is the same as that used for the SCP-mediated one-pot reaction described above.

Phylogenetic Analyses and Sequence Similarity Network Construction. A total of 43,815 representative bacterial species were selected to investigate the diversity and evolution of QbsL-like gene (AMP-ligase/C-methyl transferase). The protein sequence of a representative homologous gene (AAL65279.1) was used as the query to conduct BLASTP algorithms against the protein databases of bacteria, with an e cutoff value of 10^{-80}. 857 significant hits of were collected for subsequent phylogenetic analyses. Each alignment was generated by the L-INS-I strategy in MAFFT and trimmed by trimAL. Two sequences (WP_165679804.1; WP_165679805.1) were removed for having excessive gaps after trimming. Large-scale phylogenetic analyses were performed using an approximate maximum-likelihood method implemented in IQTREE2. Domain architectures of fused gene were annotated using InterProscan with Pfam database. 52 proteins clustered in gene tree were identified as QbsL-like fused gene of AMP-ligase/C-methyl transferase with QbsL-specific O-methyltransferase domain (PF00891).

The 857 homologous genes obtained from the above steps were subjected to pairwise BLASTP alignment to obtain E-values. E-values of pairwise sequence less than E^{-140}, and E^{-160} were used to construct the similarity network separately. Homologous genes within the gene clusters of TQB biosynthesis were obtained by using BLASTP, and genes were extracted by Seqkit. OrthoFinder was used to identify orthologous genes. Location of genes was obtained from general feature format files of the genomes.

Preparation of NaSeH. NaSeH was prepared by reducing selenium powder (Se_0) with sodium borohydride ($NaBH_4$) under nitrogen (N_2) atmosphere according to the reported method.[33] The reaction comprised 0.6 M sodium borohydride (57.5 mg) and 0.3 M selenium powder (58.5 mg), both dissolved in 2.5 mL of deionized water that had been degassed via sonication and nitrogen purging to minimize the oxygen content. After stirring at room temperature for 10 min under a nitrogen atmosphere, the solution became colorless. The reaction does not require strict anaerobic conditions, but the presence of oxygen accelerates the oxidation of NaSeH. Thus, the prepared NaSeH solution should be used immediately.

Chemoenzymatic Synthesis of dmSeQB and SeQB. The reaction system for dmSeQB and SeQB production contained 200 μM XTA, 20 mM NaSeH, 4 mM ATP, 5 mM $MgCl_2$, 2 mM SAM, 1 mM CoA 5 mM DTT and 10 μM QbsL all within a total reaction volume of 100 uL (reaction buffer: 50 mM NaH_2PO_4, 300 mM NaCl, pH = 7.4). After incubation at 30 °C for 1 h, 200 μL of methanol was added to terminate the reaction. The supernatants were analyzed using HPLC-MS with a gradient elution program following centrifugation. The HPLC program, utilizing ACN (0.1% formic

https://doi.org/10.1021/acs.jnatprod.5c00331
J. Nat. Prod. 2025, 88, 1425−1433

acid) in H_2O (0.1% formic acid), was set as follows: 0−1 min, 5%; 2−25 min, 5−60%; 25−26 min, 60−100%; 26−30 min, 100%; 30−31 min, 100−5%; and 31−35 min, 5% at a flow rate of 1 mL/min, monitoring at 254 nm. Due to the lack of available standards for SeQB and dmSeQB, their yields were estimated by comparing their HPLC peak areas to that of the substrate XTA in the negative control reaction. At 2 mM NaSeH, dmSeQB's peak area (69.95) versus XTA's (1896.03) gave a 3.69% yield; at 20 mM NaSeH, the yield increased to 13.46% (255.23/1896.03). SeQB was undetectable by HPLC, indicating a yield <1%. This calculation assumes that selenium substitution in XTA does not significantly alter its UV absorption properties.

Preparation of dmTQB and TQB. The preparation-grade reaction system for TQB and dmTQB contained 200 μM XTA, 10 mM NaSH, 4 mM ATP, 5 mM $MgCl_2$, 2 mM SAM, 1 mM CoA, 10 μM QbsL and 5 μM QbsK, all within a total reaction volume of 200 mL (reaction buffer: 50 mM NaH_2PO_4, 300 mM NaCl, pH = 7.4). After incubation at 30 °C for 2 h, 400 mL of methanol was added to terminate the reaction. The supernatant was then analyzed according to the above HPLC method, and the product was subsequently purified using the semipreparative HPLC with a Pack Pro C18 column (10 mm × 250 mm × 5 μM, YMC, Japan). The HPLC program, utilizing ACN (0.04% formic acid) in H_2O (0.04% formic acid), was set as follows: 0−1 min, 20%; 1−12 min, 20−50%; 12−12.1 min, 50−100%; 12.1−16 min, 100%; 16−16.1 min, 100−20%; and 16.1−20 min, 20%; 2.5 mL/min, monitoring at 254 nm. From 9.85 mg of starting substrate XTA, 1.4 mg of TQB (with a yield of 12.4%) and 1.6 mg of dmTQB (with a yield of 15.0%) were obtained, respectively.

NMR Data of TQB. The prepared TQB is in the form of a yellow, amorphous powder: ^{1}H NMR (600 MHz, DMSO-d_6) δ 7.56 (s, 1H), 7.56 (s, 1H), 7.51 (t, J = 7.9 Hz, 1H), 7.16 (d, J = 7.6 Hz, 1H), 4.11 (s, 3H). ^{13}C NMR (151 MHz, DMSO-d_6) δ 165.51, 163.91, 163.31, 153.53, 137.64, 129.31, 112.60, 111.58, 99.69, 56.73.

NMR Data of dmTQB. The prepared dmTQB is in the form of a yellow, amorphous powder: ^{1}H NMR (600 MHz, DMSO-d_6) δ 11.02 (s), 7.46 (s), 7.09 (s), 7.07 (s), 6.46 (s). ^{13}C NMR (151 MHz, DMSO-d_6) δ: 198.45, 160.49, 146.93, 145.41, 129,19, 126.22, 123.04, 114.86, 114.40, 103.63.

■ ASSOCIATED CONTENT

Data Availability Statement

The NMR spectroscopic data have been deposited in the Natural Products Magnetic Resonance Database (NP-MRD), with NP-CARD ID NP0351057 for TQB and NP-CARD ID NP0351059 for dmTQB. Proteins from *P. fluorescens* ATCC 17400 were retrieved from the protein database of the National Center for Biotechnology Information (NCBI) with the following accession codes: AAL65287.1 for QbsE, AAL65285.1 for QbsC, AAL65279.1 for QbsL and AAL65280.1 for QbsK. All other relevant data that supports the findings of this study are available in the article and the Supporting Information.

Supporting Information

The Supporting Information is available free of charge at https://pubs.acs.org/doi/10.1021/acs.jnatprod.5c00331.

Experimental details including tables, schemes, figures, HR-MS spectra and NMR spectra (PDF)

Bioinformatics data (XLSX)

■ AUTHOR INFORMATION

Corresponding Author

Xingwang Zhang − *Shandong Research Institute of Industrial Technology, Jinan 250101, China; State Key Laboratory of Microbial Technology, Shandong University, Qingdao, Shandong 266237, China;* orcid.org/0000-0003-1346-1183; Email: zhangxingwang@sdu.edu.cn

Authors

Xuan Wang − *State Key Laboratory of Microbial Technology, Shandong University, Qingdao, Shandong 266237, China;* orcid.org/0009-0004-9544-2887

Xiaolin Tian − *Institute of Marine Science and Technology, Shandong University, Qingdao, Shandong 266237, China*

Jiawei Guo − *State Key Laboratory of Microbial Technology, Shandong University, Qingdao, Shandong 266237, China*

Fangyuan Cheng − *State Key Laboratory of Microbial Technology, Shandong University, Qingdao, Shandong 266237, China*

Mingyu Liu − *State Key Laboratory of Microbial Technology, Shandong University, Qingdao, Shandong 266237, China;* orcid.org/0000-0001-8096-486X

Shanmin Zheng − *State Key Laboratory of Microbial Technology, Shandong University, Qingdao, Shandong 266237, China*

Yangliu Feng − *State Key Laboratory of Microbial Technology, Shandong University, Qingdao, Shandong 266237, China*

Ying Lv − *State Key Laboratory of Microbial Technology, Shandong University, Qingdao, Shandong 266237, China*

Yuanning Li − *State Key Laboratory of Microbial Technology, Shandong University, Qingdao, Shandong 266237, China*

Shengying Li − *State Key Laboratory of Microbial Technology, Shandong University, Qingdao, Shandong 266237, China; Laboratory for Marine Biology and Biotechnology, Qingdao Marine Science and Technology Center, Qingdao, Shandong 266237, China;* orcid.org/0000-0002-5244-870X

Complete contact information is available at: https://pubs.acs.org/10.1021/acs.jnatprod.5c00331

Notes

The authors declare no competing financial interest.

■ ACKNOWLEDGMENTS

This work was supported by the National Key R&D Program of China (2022YFC2804500), the National Natural Science Foundation of China (32470043, 22237004 and 323B2049), the Taishan Scholars Program (tsqn202408318), the Shandong Provincial Natural Science Foundation (ZR2023ZD50), and State Key Laboratory of Microbial Technology Open Projects Fund (M2023-01). The authors are grateful to Jingyao Qu, Guannan Lin, Jing Zhu, Zhifeng Li, Haiyan Sui and Xiangmei Ren from the State Key Laboratory of Microbial Technology at Shandong University for their guidance and assistance in HPLC, HPLC-MS and NMR analysis.

■ REFERENCES

(1) Brosnan, J. T.; Brosnan, M. E. *J. Nutr.* **2006**, *136*, 1636S−1640S.
(2) Zhao, C.; Rakesh, K. P.; Ravidar, L.; Fang, W.-Y.; Qin, H.-L. *Eur. J. Med. Chem.* **2019**, *162*, 679−734.
(3) Haque, N.; Parveen, S.; Tang, T.; Wei, J.; Huang, Z. *Mar. Drugs* **2022**, *20*, 528.
(4) Dunbar, K. L.; Scharf, D. H.; Litomska, A.; Hertweck, C. *Chem. Rev.* **2017**, *117*, 5521−5577.
(5) Wang, N.; Saidhareddy, P.; Jiang, X. *Nat. Prod. Rep.* **2020**, *37*, 246−275.

(6) Matthijs, S.; Baysse, C.; Koedam, N.; Tehrani, K. A.; Verheyden, L.; Budzikiewicz, H.; Schäfer, M.; Hoorelbeke, B.; Meyer, J. M.; De Greve, H.; Cornelis, P. *Mol. Microbiol.* **2004**, *52*, 371−384.
(7) Dong, L.-B.; Rudolf, J. D.; Kang, D.; Wang, N.; He, C. Q.; Deng, Y.; Huang, Y.; Houk, K. N.; Duan, Y.; Shen, B. *Nat. Commun.* **2018**, *9*, 2362.
(8) Lewis, T. A.; Cortese, M. S.; Sebat, J. L.; Green, T. L.; Lee, C.; Crawford, R. L. *Environ. Microbiol.* **2000**, *2*, 407−416.
(9) Sebat, J. L.; Paszczynski, A. J.; Cortese, M. S.; Crawford, R. L. *Appl. Environ. Microbiol.* **2001**, *67*, 3934−3942.
(10) Xue, D.; Zou, H.; Qiu, Y.; Lv, W.; Madden, M. D.; Xu, M.; Lian, X.; Pulliam, C.; Older, E. A.; Hou, L.; Campbell, A.; De Rond, T.; Awakawa, T.; Yuan, C.; Moore, B. S.; Li, J. *Nat. Chem.* **2025**, DOI: 10.1038/s41557-025-01833-9.
(11) Barry, S. M.; Challis, G. L. *Curr. Opin. Chem. Biol.* **2009**, *13*, 205−215.
(12) Thrane, C.; Jensen, D. F.; Tronsmo, A. *Eur. J. Plant Pathol.* **2000**, *106*, 215−225.
(13) Paulitz, T. C.; Bélanger, R. R. *Annu. Rev. Phytopathol.* **2001**, *39* (1), 103−133.
(14) Matthijs, S.; Tehrani, K. A.; Laus, G.; Jackson, R. W.; Cooper, R. M.; Cornelis, P. *Microbiol.* **2007**, *9*, 425−434.
(15) Godert, A. M.; Jin, M.; McLafferty, F. W.; Begley, T. P. *J. Bacteriol.* **2007**, *189*, 2941−2944.
(16) Wessjohann, L. A.; Schneider, A.; Abbas, M.; Brandt, W. *Biol. Chem.* **2007**, *388*, 997−1006.
(17) Álvarez-Pérez, M.; Ali, W.; Marć, M.; Handzlik, J.; Domínguez-Álvarez, E. *Molecules* **2018**, *23*, 628.
(18) Sonego, J. M.; de Diego, S. I.; Szajnman, S. H.; Gallo-Rodriguez, C.; Rodriguez, J. B. *Chem.—Eur. J.* **2023**, *29*, No. e202300030.
(19) Sonawane, A. D.; Koketsu, M. *Curr. Org. Chem.* **2020**, *23*, 3206−3225.
(20) Kageyama, H.; Murai, T.; Kanda, T.; Kato, S. *J. Am. Chem. Soc.* **1994**, *116*, 2195−2196.
(21) Kato, S.; Kageyama, H.; Takagi, K.; Mizoguchi, K.; Murai, T. *J. Prakt. Chem.* **1990**, *332*, 898−910.
(22) Kayrouz, C. M.; Huang, J.; Hauser, N.; Seyedsayamdost, M. R. *Nature* **2022**, *610* (7930), 199−204.
(23) Zhang, X.; Cheng, F.; Guo, J.; Zheng, S.; Wang, X.; Li, S. *Nat. Synth.* **2024**, *3*, 477−487.
(24) Alphafold2 server: https://github.com/deepmind/alphafold.
(25) Beuerle, T.; Pichersky, E. *Arch. Biochem. Biophys.* **2002**, *400*, 258−264.
(26) Stuible, H.-P.; Kombrink, E. *J. Biol. Chem.* **2001**, *276*, 26893−26897.
(27) Oba, Y.; Ojika, M.; Inouye, S. *FEBS Lett.* **2003**, *540*, 251−254.
(28) Schubert, H. L.; Blumenthal, R. M.; Cheng, X. *Trends Biochem. Sci.* **2003**, *28*, 329−335.
(29) Alphafold3 server: https://www.alphafoldserver.com.
(30) Struck, A. W.; Thompson, M. L.; Wong, L. S.; Micklefield, J. *ChemBioChem.* **2012**, *13*, 2642−2655.
(31) Sazinas, P.; Hansen, M. L.; Aune, M. I.; Fischer, M. H.; Jelsbak, L. *Genome Biol. Evol* **2019**, *11*, 3529−3533.
(32) Cornelis, P. *Appl. Microbiol. Biotechnol.* **2010**, *86*, 1637−1645.
(33) Klayman, D. L.; Griffin, T. S. *J. Am. Chem. Soc.* **1973**, *95*, 197−200.

https://doi.org/10.1021/acs.jnatprod.5c00331
J. Nat. Prod. 2025, 88, 1425−1433